ELSEVIER

Marine Geology 211 (2004) 143–168

MARINE GEOLOGY
INTERNATIONAL JOURNAL OF MARINE GEOLOGY, GEOCHEMISTRY AND GEOPHYSICS

www.elsevier.com/locate/margeo

Types of internal structure and external morphology of submarine dunes under the influence of tide- and wind-driven processes (Dover Strait, northern France)

Sophie Le Bot[a,*], Alain Trentesaux[b]

[a]*UMR CNRS 6143, Morphodynamique continentale et côtière, Université de Rouen, Département de Géologie, 76821 Mont Saint Aignan Cédex, France*

[b]*UMR CNRS 8110 PBDS, FR 1818, Université des Sciences et Technologies de Lille, SN5, 59 655-Villeneuve d'Ascq Cédex, France*

Received 14 August 2003; received in revised form 28 May 2004; accepted 2 July 2004

Abstract

The expression of tide- and wind-driven processes in the internal architecture and external morphology of very large submarine dunes is investigated at a dune field located in the central part of the Dover Strait (Southern North Sea). Current measurements and sediment transport calculations enable quantification of the dominant tide- and wind-driven processes, and very high resolution seismic recordings are used to analyse internal structure and external morphology of dunes.

In the study area, moderate to storm winds induce temporary currents that can lead to the reversal of sediment transport direction and induced erosive processes on the seabed. Dune master-bedding consists of extended erosive surfaces with 9–11° slopes that bound storm-generated sets of cross-beds, 1.5–4.85 m thick (2.65 m on average). Three types of architectures are observed within the dune field, and occasionally within single dunes. These types, which display a strong linkage between internal structure and external morphology, consist of: (1) asymmetric dunes with cosets, which dip in the direction of the marked external asymmetry of the dunes; (2) dunes with a complex external morphology composed of mega-herringbone structures, each displaying an opposing progradation direction; and (3) dunes with a symmetric megaripple bedding unit at their summit. The diversity of the internal architecture and external morphology results from the variable combinations of tide- and wind-driven processes occurring in the study area. The asymmetry of tidal peak current velocity and the relative strength of wind-driven currents are the parameters that have the most important influence on dune architecture. Asymmetric dunes with cosets result from a strong asymmetry in tidal peak current velocity, which is reversed only slightly during storms. Dunes with mega-herringbone structures and dunes with symmetric megaripple units at their summit are observed in areas where the asymmetry of the tidal peak current velocity is negligible, allowing reversal of the sediment transport and dune migration directions each time moderate winds blow. The latter architectural type is specific to sand-rich areas.

The different dune architecture types display strong geometrical similarities to structures observed in dunes from other shelf environments where driving processes are different. This implies that a study based only on a geometric description of internal structures will not enable the reconstitution of ancient depositional environments. A better discriminant criteria seems to be the

* Corresponding author.
E-mail address: sophie.lebot@univ-rouen.fr (S. Le Bot).

doi:10.1016/j.margeo.2004.07.002

thickness of the second-order sets of cross-beds which is correlated with specific hydro-sedimentary processes. Dune height also probably has an important influence on the thickness of second-order sets of cross-beds, as dune height and set thickness display a clear relationship in the present study.

Keywords: submarine dune; tide- and wind-driven processes; storms; seismics; internal structure; southern North Sea

1. Introduction

Characterisation and interpretation of the internal structure of submarine dunes is still a matter of discussion. In tidal environments, several models of dune architecture have been proposed. Although they display strong geometric similarities, the genetic processes proposed for the formation of the internal bounding surfaces and the global architecture vary. According to Allen (1980), the degree of asymmetry within the internal structure of the dune and the external morphology both are controlled by tidal current velocity instability and asymmetry. From direct observations of intertidal dunes, Dalrymple (1984) stressed the fact that superimposed dunes play a key-role in the dynamics and internal structure of the host dune. From very high resolution seismic data and cores, Berné (1991) and Berné et al. (1988, 1989, 1993) concluded that dune master-bedding, in several shallow areas along the French continental shelf, consists of bounding surfaces formed during episodic or seasonal non-tidal events (e.g., variations in river discharge in the Gironde Estuary, southwestern France; wave climate in the Bay of Bourgneuf, western France).

On epicontinental shelves, tides are generally the main agents responsible for sediment transport and bedform migration, but wind-driven currents can also play an important role, for example, in the seasonal inversion of dune polarity (Harris, 1989, 1991; Thauront et al., 1996). In the Dover Strait, large dunes display changing migration rates and directions according to the wind regime and the storm activity (Le Bot et al., 2000; Le Bot, 2001).

The main objective of this paper is to establish the relation between tide- and wind-driven processes and their signature in the internal structure and external morphology of subtidal dunes. Knowledge of the formation and evolution mechanisms of sedimentary bedforms can be improved by studying their internal structure, within which the distinct building stages of dunes are recorded. The internal structure of the dunes displays bounding surfaces which are typical of specific hydro-sedimentary processes. Recognition of such structures in the stratigraphic record may enable the reconstitution of ancient depositional environments and processes. This would be of special interest in areas where deposits are scarse and thin or concentrated mainly in bedforms (e.g., the present-day Dover Strait area; James et al., 2002).

2. Study area

The study area consists of a field of submarine dunes, located in the central part of the Dover Strait at the southern extremity of the South Falls sandbank. The water depths range from 20 to 40 m (Fig. 1).

2.1. The Dover Strait

The Dover Strait corresponds to a shallow water continental shelf, where tidal currents are the main agents responsible for sediment dynamics. This strait is characterised by semi-diurnal tides and macrotidal conditions. In the dune field, mean neap tidal range is 2.7 m and mean spring tidal range is 5.7 m. Given the constriction of the basin, tidal currents are rectilinear, with an ellipse eccentricity of 0.03, and their intensity increases to a maximum in the middle of the strait. During the flood and ebb phases, which flow towards the NE and the SW, respectively, currents reach 1.65 and 1.85 m/s at the sea surface during mean spring

Fig. 1. Study area. (I) Bathymetric map of the Dover Strait with location of the dune field (from James et al., 2002); (II) detailed water depth in the study area (multibeam data: dunes f–p, 1995, dunes a–e, 1999; single-beam data: dunes o′ –u, 1999), and location of submarine dunes, current measurements and sediment samples with grain-size analysis.

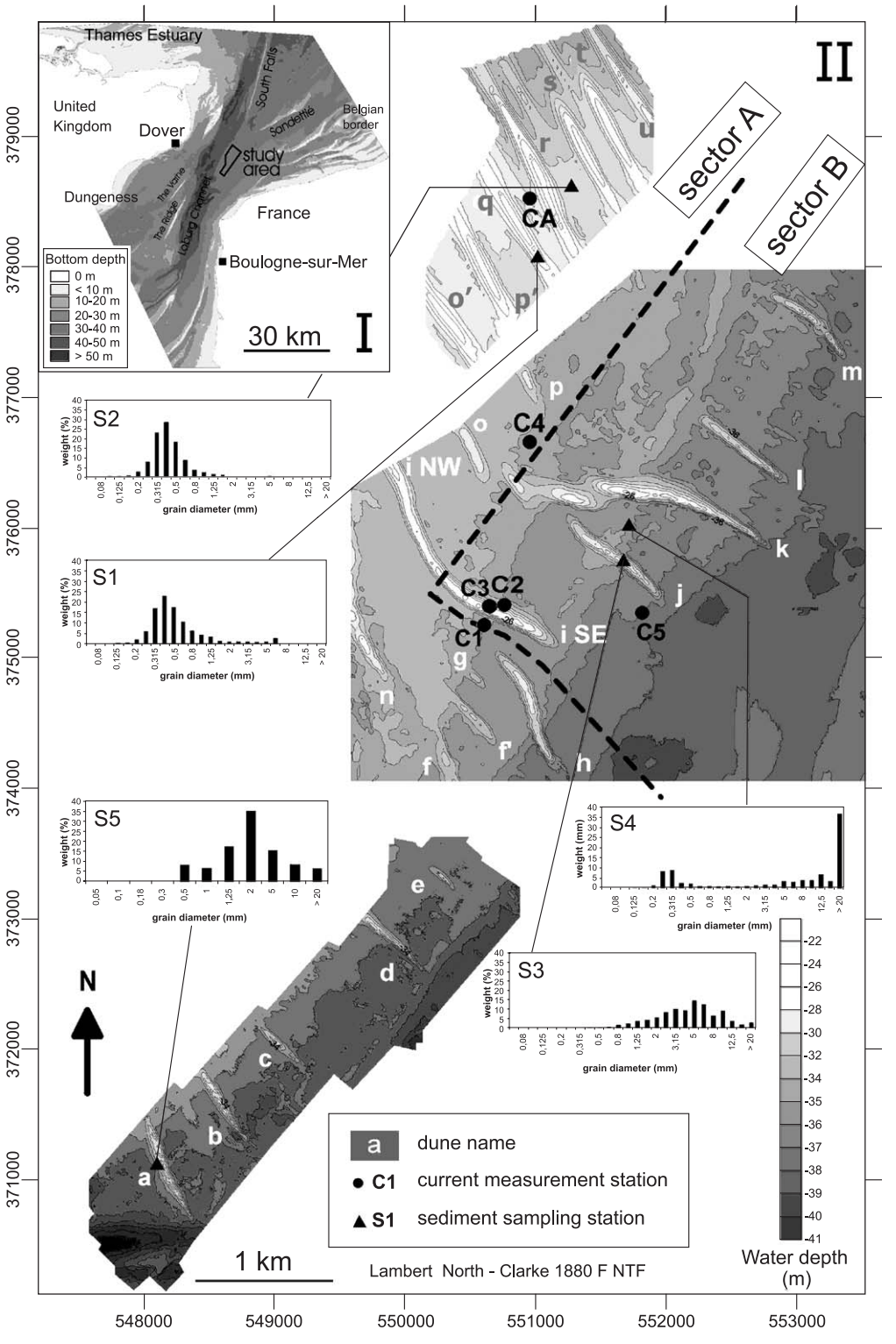
Thames Estuary
South Falls
United Kingdom
Dover
sandbank
Belgian border
study area
Dungeness
The Varne
The Ridge
Goodwin Channel
France
Boulogne-sur-Mer
Bottom depth
0 m
< 10 m
10-20 m
20-30 m
30-40 m
40-50 m
> 50 m
30 km
I
II
sector A
sector B
CA
C1
C2
C3
C4
C5
S1
S2
S3
S4
S5
weight (%)
weight (mm)
grain diameter (mm)
N
1 km
a dune name
C1 current measurement station
S1 sediment sampling station
Lambert North - Clarke 1880 F NTF
Water depth (m)
379000
378000
377000
376000
375000
374000
373000
372000
371000
548000
549000
550000
551000
552000
553000

tides (SHOM, 1968). Winds also are important hydrodynamic agents in the Dover Strait. They are funneled when crossing the strait and blow essentially from SW (30.5% from N170° to N260°) and NE (16% from N350° to N80°) provenances. The long-term water flux is due half part to wind-induced currents (Prandle, 1993) and presents seasonal variability linked to sensitivity to wind (Salomon et al., 1993).

In the southern North Sea and the Dover Strait, sand transport pathways fit the pattern of peak bottom stress, rather than the average value over a tidal cycle, and do not fit the pattern of residual flows (Pingree and Griffiths, 1979). In the central part of the strait, residual sediment transport is oriented in the peak ebb direction over a long-term basis (Beck et al., 1991; Grochowski et al., 1993), but can be reversed by seasonal variations in moderate winds or storm wave directions (Grochowski et al., 1993). This transport pathway begins at a bedload parting between the city of Calais and the Wash estuary, and ends at a convergence zone in the southwestern part of the strait (Kenyon et al., 1981; Johnson et al., 1982; Beck et al., 1991; Grochowski et al., 1993; Harris et al., 1995).

Acceleration of the current as it approaches the strait prevents the deposition and preservation of sand and gravel. The seabed is composed essentially of a relict pebble-lag pavement, some tens of cm thick, deposited by large Pleistocene fluvial systems prior to the post-glacial sea-level rise (Houbolt, 1968; Jelgersma, 1979). The pebble lag pavement is mantled with a series of scarce sand and gravel bedforms, mainly represented by dunes and sandbanks (James et al., 2002).

2.2. The dune field

In the study area, the dunes are found in two groups (Fig. 1): one group to the SE with 14 dunes (dunes a–m) and a second group to the NW with 11 dunes (dunes i NW and n–u). Dune i, the largest in the study area, belongs to both groups. The dunes display heights between 4 and 12.5 m and wavelengths ranging from 200 to 1100 m. These correspond to very large compound dunes, covered with small- to medium-sized superimposed dunes. The dune field can be divided into two sectors, A and B (Fig. 1), comprising dunes that present various morphodynamic characteristics previously analysed by Le Bot et al. (2000) and Le Bot (2001).

2.2.1. Sector A

This sector constitutes the relict extremity of the South Falls sandbank and is now subject to active erosion (Le Bot, 2001) similar to that seen on the sandbank itself (Smith, 1988). The dunes are typical of sand-rich environments and low energy hydrodynamics (Le Bot, 2001). They consist of small to very large dunes organised in a compact field and presenting homogeneous 2D morphologies. In the northern part (dunes i NW and n–u), they consist of a medium sand (samples S1 and S2, Fig. 1) with a common 0.35-mm mode, totally covering the pebble lag. The sand mainly originates from the erosion of the South Falls and Sandettié sandbanks (Smith, 1988). In the southern part (dunes a–h), the dunes are composed of a mixture of sand to shelly gravel (sample S5, Fig. 1); they lie on the pebble lag mantled with an heterogeneous thin sand and gravel cover, which is mainly moulded in smooth to rippled sand ribbons. In sector A, dune migration is variable in direction and rate depending on the wind regime and the time-scale at which the observations are recorded (Le Bot et al., 2000; Le Bot, 2001).

2.2.2. Sector B

Dunes g to m are typical of sand-starved environments and high energy hydrodynamic regimes (Le Bot, 2001). They comprise very large, isolated three-dimensional dunes, which frequently lack superimposed smaller dunes. They are composed of a coarse heterogeneous sediment, made of flattened shelly gravels of mode 2.5–10 mm at the crest of the dune (sample S3, Fig. 1), becoming bimodal on the dune flanks when associated with 0.35-mm medium sand. Between the dunes, pebbles largely occurring in the strait are associated with a small volume (less than 10%) of 0.35-mm medium sand (sample S4, Fig. 1). Repeated bathymetric surveys indicate that dunes from sector B migrate always towards the SW (Le Bot et al., 2000; Le Bot, 2001).

3. Hydro-sedimentary processes

Results from current measurements (Le Bot, 2001; Idier, 2002a,b) and hydrodynamic modelling (Idier, 2002a,b) are used to quantify the characteristics of hydro-sedimentary processes acting on the dunes. Special attention has been paid to instantaneous and

residual sediment transport caused by tidal currents, solely, and to combined tide- and wind-driven currents.

3.1. Combination of tides and winds. Example of current measurements, 1999

A current measurement campaign was undertaken by MHA-SHOM (Hydrographic Mission of the Atlantic Ocean-French Naval Hydrographic and Oceanographic Office) in September and October 1999, using an Aquadopp acoustic Doppler current meter. Measurements correspond to 10 mn averages of currents that were recorded during 1 min at a frequency of 1 Hz (Fig. 2). Measurements were made over 13.3 days, 1 m above the flat seabed in the northern part of sector A between dunes q and r (station CA, location in Fig. 1). Low neap conditions prevailed at the beginning and the end of the measurement period, and high spring conditions in the middle (Fig. 2b).

3.1.1. Currents

Current roses established from the measurements indicate rectilinear, nearly equivalent flood and ebb peak current velocities (Fig. 2e). In mean spring and mean neap conditions, these velocities reach 1.31 and 0.93 m/s, respectively, in N29° direction during the flood phase, and 1.28 and 0.85 m/s, respectively, in N216° direction during the ebb phase. The flood and ebb phases display a low peak velocity asymmetry of 0.03–0.08 m/s in favour of the flood, which is negligible compared to instantaneous peak current velocities (tidal peak current velocity asymmetry corresponds to the difference between flood peak and ebb peak velocities). Globally, the signature of the semi-lunar cycle can be seen in the record of instantaneous current velocities (Fig. 2b and c). However, strong variations occur in the flood–ebb relative peak velocities, especially under neap conditions. They cannot be produced by tide only. Analysis of residual currents provides more insight into the causes of these variations (Fig. 2d and f).

Cumulative current vectors are reported in Fig. 2d. The figure shows the course that a water particle would take if it was dropped at the gauging station and followed the currents measured at this station. This Lagrangian representation of an Eulerian parameter, which is carried out by considering a current to be uniform over the study area, gives a qualitative evaluation of the water mass displacement. It enables to see the semi-diurnal current oscillation and highlights the existence of residual currents. Fig. 2f shows the direction and velocity of the residual currents. They are calculated by subtracting the predicted current from the observed one and by applying tide-frequency filters that enable an elimination of the diurnal and semi-diurnal frequencies. Periods with distinct residual current characteristics can be delimited. Several periods display residual currents in the strait axis direction: (1) from 22 to 25 September residual currents reach velocities of 0.22 m/s towards N20°, (2) from 1 to 3 October they reach speeds of 0.37 m/s towards N25°, and (3) from 3 to 5 October they reach speeds of 0.40 m/s towards the N220°. However, global residuals are oriented through-strait (Fig. 2d); this is particularly visible between 25 September and 1 October where the residuals have velocities from 0.13 to 0.20 m/s, fluctuating from N320° to N15° (Fig. 2f), with an overall N350° direction (Fig. 2d).

During the period over which the current was measured, wind speeds, recorded in Boulogne-sur-Mer,[1] were moderate (3–12 m/s), from the S–SW (mainly N180–220°) between 22 and 24 September, turning progressively SW (mainly N200–N240°) between 24 and 3 October, then drastically N–NE (mainly N310–340°) between 4 and 5 October (Fig. 2a). There is a strong correlation between wind and current characteristics (Fig. 2a,c,d,f). Some periods of current measurement can be considered as representative of "pure" tidal conditions during which winds have a negligible influence, while others are typical of combined tide and wind conditions:

(1) Between 25 September and 1 October, mean to high spring tides are observed, associated with weak winds (5–12 m/s), which have little effect on tidal currents. Flood and ebb peak velocity asymmetry is 0.05 m/s and the water mass displays a residual displacement equivalent to 9.5 km/day in a N–NW (N350°) direction. The

[1] Wind data are not recorded in the strait, but rather in Boulogne-sur-Mer (location in Fig. 1), the coastline of which is N–S-oriented. Due to the geographic configuration, N winds in Boulogne-sur-Mer generally correspond to NE winds in the Dover Strait.

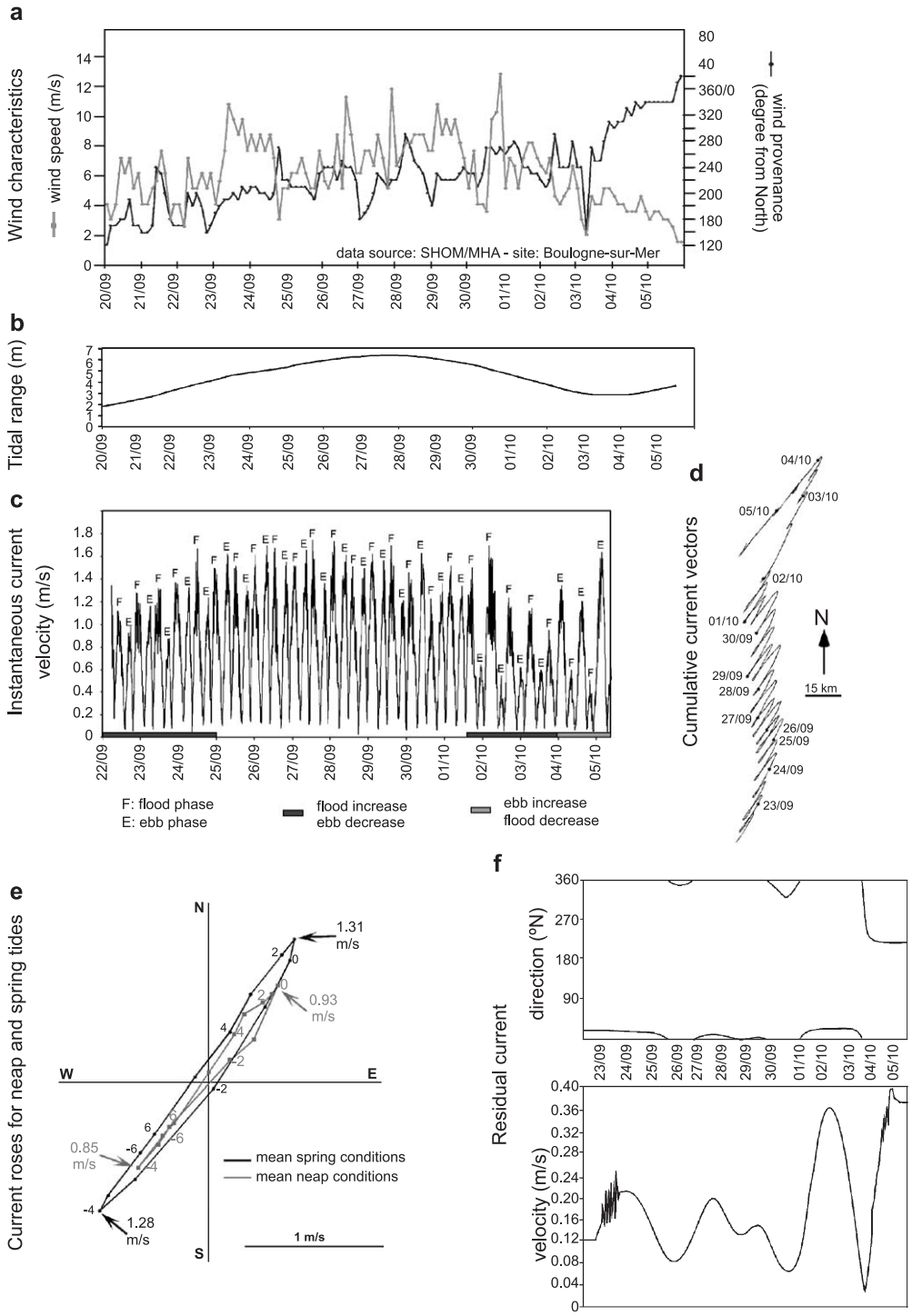

Fig. 2. Current and wind parameters recorded between 22 September and 5 October 1999. (a) Wind directions and speeds recorded at Boulogne-sur-Mer; (b) tidal range; (c, d, e, f) current characteristics recorded at station CA (1 m above the seabed, location Fig. 1): (c) instantaneous current velocities; (d) cumulative current vectors; (e) current roses for mean neap and mean spring tide (numbers ranging from − 6 to 6 correspond to time, in hours, before and after high tide in the harbour of Calais); (f) residual currents (after tide-frequency filtering): velocity and direction characteristics.

N–NW residuals indicate a through-strait non-oscillatory flow component, previously reported by Jones et al. (1994) 4 km from Gris-Nez Cape. This component probably is not induced by winds, as it is orientated perpendicular to wind directions, but rather is tide-generated.

(2) During neap to mean tides, strong variations of the flood and ebb current instantaneous velocities and peak velocity asymmetry have been observed, as well as strong residual currents in the strait axis direction. These variations correlate well with wind characteristics, and therefore are assumed to be induced by the action of superimposed wind-driven currents. Under the influence of moderate SW winds (3–12 m/s), flood strength is increased and ebb strength is decreased. Peak current velocity asymmetry is largely increased in favour of the flood, up to 0.30 m/s from 22 to 25 September, and up to 1.14 m/s from 1 to 4 October. During these periods, residual currents are oriented towards the N–NE (N20°) and reach mean velocities of 0.2 and 0.36 m/s, respectively. Global residual displacements are about 46 km towards N20° between 22 and 25 September and 67.5 km towards N25° from 1 to 4 October. Conversely, under the influence of moderate northerly winds, the peak current velocity asymmetry is reversed in favour of the ebb and reaches up to 0.75 m/s on 4 and 5 October. The residual currents are orientated towards the SW (N220°) with a mean velocity of 0.38 m/s, and a residual displacement of 53.25 km is observed in this direction.

3.1.2. Sediment transport

Given the particle size range at the current measurement station (samples S1 and S2, Fig. 1), sand is mobilised as bedload for a critical friction velocity (u_*) of 1.5×10^{-2} m/s (Miller et al., 1977), and as suspended load for a critical friction velocity of 4.08×10^{-2} m/s, calculated using Bagnold's criteria:

$$u_* \geq W_s/1.25 \quad (1)$$

where W_s is the settling velocity, equal to 5.1×10^{-2} m/s for 0.35-mm quartz grains (Baba and Komar, 1981).

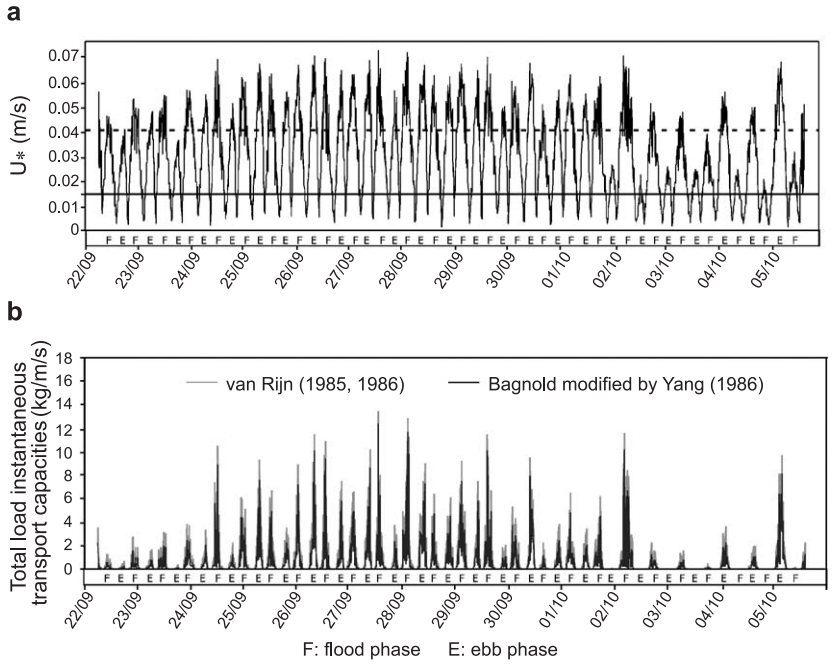

Fig. 3. Sediment transport characteristics calculated from currents recorded at station CA. (a) Friction velocities (u*) for a 0.35-mm quartz sand (continuous line: bedload critical friction velocity; broken line: suspended load critical friction velocity); (b) total load instantaneous transport capacities, quantified using the formulas from Bagnold modified by Yang (1986) and van Rijn (1985, 1986).

Friction velocity is calculated from the current measurement by assuming a logarithmic velocity profile for the first metre above the seabed, described by the von Karman–Prandtl's equation (Dyer, 1986). The bedload criteria is reached for each tidal current phase, in high spring tides as well as during low neap tides, with the exception of about 1 h at each tidal current reversal period (Fig. 3a). The suspension criteria is satisfied during several hours of flood and ebb phases in spring conditions, and during one of the flood or ebb peak phase in neap conditions, especially when this phase has been reinforced by winds (e.g., ebb peak phase on 4 and 5 October, Fig. 3a).

Total transport capacities have been calculated from the current measurements, using two formulas: Bagnold's formula modified by Yang (1986) and van Rijn's formulas (1985, 1986)(Fig. 3b). The first formula provided the best results for a dune field in the English Channel (northern France), where the hydrodynamic setting is similar to the one observed in the present study (Berné, 1991), and the van Rijn's formulas for the Dover Strait (Grochowski et al., 1993). Values of total transport capacities calculated with the two formulas are similar being about 1.3 times higher with the van Rijn's formulas. The suspended load represents no more than 6–8% of the total transport load (Le Bot, 2001). In the case of "pure" tidal conditions on 27 September, instantaneous total transport capacities for the highest tide (tidal range: 6.36 m) corresponded to 1.24–1.35 kg/m/s during the flood peak, and 0.87–1.02 kg/m/s during the ebb peak. In the case of combined tide and wind conditions, sediment transport was highly variable. On 23 September, for a mean tide, the S–SW winds (N190–210°, 8–11 m/s) resulted in an increase in transport capacity during the flood peak (0.19–0.32 kg/m/s) and in a decrease during the ebb peak (0.08–0.16 kg/m/s). Between 1 and 4 October, in mean to neap tidal conditions, the winds were weaker (4–8 m/s), but more parallel to the tidal currents (N200°–N240°). During this period, sediment transport reversal did not occur: no transport was observed during ebb phases, whereas the flood transport was equivalent to total transport capacities reached during mean spring tide conditions (Fig. 3b). On 4 and 5 October, the opposite situation was observed under the action of N winds.

During the entire current measurement period, total residual transport capacity corresponds to 860–1340 kg/m/day towards the N (N12°). Under "pure" tidal conditions, this transport capacity is estimated to be 1200–1850 kg/m/day towards N16°. When moderate winds blow during neap conditions, residual transport capacity is tripled (2450–3970 kg/m/day towards N31° between 1 and 4 October, and 2770–4450 kg/m/day towards N222° between 4 and 5 October).

3.2. Hydro-sedimentary characteristics in sectors A and B

From the analysis of dune migration at monthly to decennial time-scales, a contrasting pattern of tidal currents between sectors A and B has been interpreted as resulting from the influence of the South Falls and Sandettié sandbanks (Le Bot, 2001). These sandbanks are 30-m high sedimentary structures, the summit of which is less than 7 m below the water surface. The sandbanks act as barriers that disturb the tidal wave propagation. They form a large funnel in which the ebb current, channelized from the NE (van Veen, 1936), is accelerated up to the SW outlet (Burton, 1977). Sector A, located at the SW extremity of the South Falls sandbank, is protected from this strong ebb current, whereas sector B, located 6 km downstream, is affected by this strong ebb current. In sector A, dune migration is variable, whereas in sector B, dune migration is observed to always be towards the SW (Le Bot et al., 2000; Le Bot, 2001). In sector A, same authors indicate that: (1) on a decennial time-scale, dunes migrate towards the NE in the direction of the flood, which is the slightly dominant tidal phase in this sector; and (2) on shorter time-scales, dune migration is correlated with wind regime, i.e., dunes migrate towards the SW or NE according to the predominant SW or NE wind-driven currents.

The work of Idier (2002a,b) and Idier et al. (2002) provides information on the hydrodynamic and sediment transport patterns, using a 2DH hydrodynamic numerical modelling and current measurements. Their results are consistent with our observations and the assumed hydrodynamical scheme.

The model predicts the regional depth-averaged tidal currents in mean spring conditions in the Dover Strait, between Dungeness, Boulogne-sur-Mer, the Thames estuary and the Belgian border (Idier,

2002a,b).[2] The large spatial extent and the grid size, down to 60 m in the dune field, was chosen to give a good representation of the morphology of the South Falls and Sandettié sandbanks (Idier, 2002a,b). The direction of the tidal residual sediment fluxes have been estimated from the cubic depth-averaged current velocities (sediment transport capacities are proportional to cubic current velocities), calculated with a 5-mn temporal sampling and integrated over a tidal cycle (Idier, 2002a,b). Idier (2002a,b) shows that these directions do not correlate with the directions of the tidal residual currents as previously observed by Pingree and Griffiths (1979). Tidal residual circulation cells have been proposed (Fig. 4, from Idier, 2002a).

From modelling results (Idier, 2002a,b) and current measurements performed by MHA-SHOM in 2001 (stations C1, C2, C3, C4 and C5, location in Fig. 1) under storm conditions (Idier, 2002b; Idier et al., 2002), the following conclusions can be drawn:

(1) In sector A, in the northern part (dunes i NW and n–u), the tidal peak current velocity asymmetry is low, as observed at station CA, and tidal residual circulation and sediment flux are not in the direction of tidal currents but rather are perpendicular to them, towards the W–NW. In the southern area of sector A (dunes a–h), the results of the numerical model indicate that the tidal residual sediment flux is weak and giratory, oriented towards the SW or the NE. Two specific features are observed (Fig. 4): a recirculation cell (gyre) between cells 2 and 3 where dunes e, f, f′ and h are located, and a convergence zone around dunes n, i SE and j.

(2) In sector B, tidal peak velocity asymmetry is strong (e.g., 0.44 m/s at stations C2 and C3, Idier, 2002b) and the tidal residual flux is strong and orientated towards the SW in the direction of the dominant ebb (Fig. 4). When NE storm conditions occur, in neap tides, winds can generate a SW wind-driven component of flow (e.g., 0.8 m/s at station C1, Idier et al., 2002) that is much stronger than the flood component and induces a non-reversal of tides, whereas this phenomena does not occur during spring tides. The dune sediment is transported as bedload during spring tides only, always in a SW direction (Idier, 2002b).

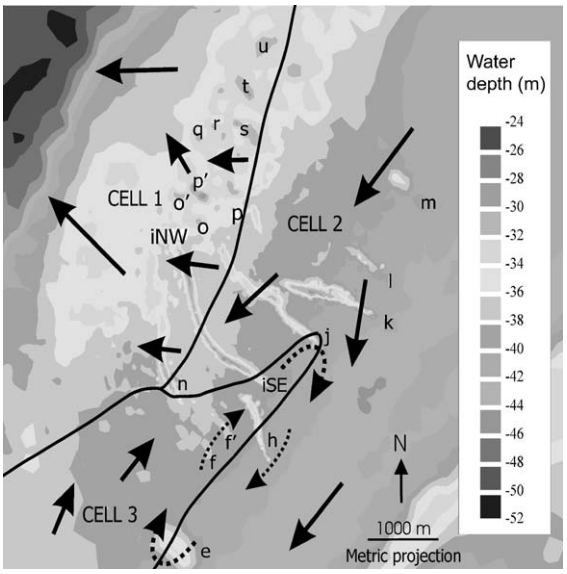

Fig. 4. Residual sediment circulation cells for a mean spring tide (from Idier, 2002a). Cells and directions are interpreted from the cubic current velocity field (grid size: 100 m), calculated with a 5-mn sampling and then integrated over a semi-diurnal tidal cycle. Solid lines: boundaries between circulation cells; arrows: directions of residual circulation (no strength information); dashed arrows: giratory circulations.

In summary, some conclusions can be drawn from this study and the works of Idier (2002a,b) and Idier et al. (2002). Wind speeds required for the cancellation of tidal peak velocity asymmetry or the non-reversal of tidal currents are more often reached in sector A than in sector B. In sector A, tidal circulation is easily modified by winds of moderate speeds (a few m/s) since tidal peak velocity asymmetry is weak (0.03–0.08 m/s) and tidal residuals are orientated N–NW, perpendicular to tidal current directions. Currents induced by moderate winds can reach speeds 10 times greater (e.g., 0.40 m/s towards the SW from 4 to 5 October at station CA) than the tidal peak velocity asymmetry. In sector B, tidal peak velocity asymmetry is strong (e.g., 0.44 m/s in mean spring conditions at stations C2 and C3) and only storm wind-driven currents occurring during neap tides modify the tidal hydrodynamic regime.

[2] Coriolis strength is taken into account, a constant viscosity is used in the turbulence model (10–4 $m^2\ s^{-1}$), and a uniform Chezy coefficient (70 $m^{1/2}\ s^{-1}$) is assumed. The model was validated by comparing 11 maregraphic stations and 44 current measurements with the model results.

Sediment transport also displays a different pattern in sectors A and B. In sector A, dune sediment is transported during both tidal phases, and the transport pattern is modified with winds: the transport is oriented towards the NE when there is either no wind or SW winds, and towards the SW when there are NE winds. In sector B, sediment transport occurs only during ebb and sediment is always transported towards the SW.

4. Internal architecture and external morphology

4.1. Seismic data acquisition

In previous studies, very high resolution seismic profiles, processed and validated using shallow coring, have been used successfully to image the internal structure of subtidal dunes (e.g., Berné et al., 1988, 1989, 1993) and tidal sandbanks (e.g., Trentesaux et al., 1999).

In this study, a 3.5-kHz EDO-Western subbottom profiler was deployed during the Ridens I (June 1996) and Ridens II (November 1998) surveys. In June 1996, 21 profiles were acquired over a total length of 88 km: 17 in a NE–SW direction, perpendicular to the dune crestlines, and 4 in a NW–SE direction. In November 1998, a total of 90 km of profiles were acquired, including 11 profiles at the same location as in 1996 and 7 complementary ones. The location of the profiles is shown in Fig. 9. The seismic system allows an efficient penetration of about 10 m, depending on the nature of the sediment and in particular grain-size. The dunes, composed of gravel and sand, are mostly insonified. The vertical resolution of the seismic data is about 0.5 m, with a blind area of 1.25 m under the water–sediment interface, caused by a strong impedance contrast and a ringing effect that is attenuated within the upper layers. The data have not been post-processed and coring attempts for validation failed due to sediment coarseness and current velocity.

4.2. Internal bounding surfaces: typology, nature and origin

4.2.1. Types of bounding surfaces

Seismic analysis of dune structure reveals a hierarchy of bounding surfaces of three different types. Given the geometric similarities the terminology defined by Brookfield (1977, 1992) in aeolian dunes and used by Berné (1991) and Berné et al. (1988, 1989, 1993) in subtidal dunes has been adopted to describe the observed bounding surfaces. The different types of surfaces are presented on the seismic section carried out on dune j (Fig. 5, location in Fig. 9).

First-order surfaces correspond to sub-horizontal reflectors. These surfaces can be attributed to two types of phenomena, as previously suggested by Berné (1991): (1) at the dune base, the surfaces display a strong reflectivity. They underline the progradational surface of the dunes above the pebble lag pavement, (2) at the dune summit, these surfaces constitute erosive levels which cut the oblique underlying reflectors. They result from erosion generated by the overlapping of smaller superimposed dunes that migrate faster than the host dune.

Second-order surfaces constitute the dune master-bedding. They dip with an angle of 9–11°, in a direction perpendicular or slightly oblique (up to 13°) to the dune crest (Le Bot, 2001). These values are similar to those obtained by Berné (1991), which range between 5° and 15°. Second-order surfaces cut the underlying units. These surfaces reflect erosive processes affecting either the progradating lee flank (e.g., dune j, Fig. 5) or the stoss side of the dunes. They delimit second-order sets of cross-beds.

Third-order surfaces correspond to the reflectors the most inclined (25–30°). They are seldom observed along the profiles given the strong diffraction resulting from their steepness, the accuracy of the system receiver (especially in this coarse material), and the absence of profile processing. According to Berné (1991), these oblique cross-beds are composed of stacked sandy beds with contrasting grain-sizes sometimes showing sorting, and are considered to result from the alternation of avalanche phases and “sandy rainfalls”.

4.2.2. Origin of second-order surfaces

In the study area, hydrodynamic agents influencing sediment transport are multiple and generally combined (see Section 3). In order to better constrain the erosive processes which give rise to second-order surfaces, the formation periodicity of these surfaces has been estimated.

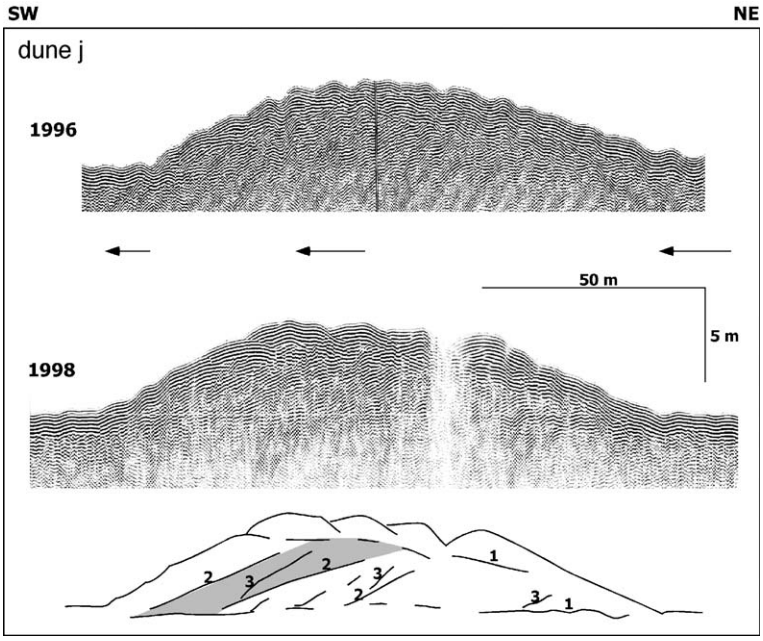

Fig. 5. Internal bounding surfaces in dune j. SW–NE seismic sections perpendicular to the crest of dune (profile 9, 1996; profile IX, 1998) and interpretation (profile IX, 1998). Location of the seismic section in Fig. 9. 1, 2, 3: first-, second-, third-order discontinuities. Shaded area: surface of sediment trapped within a recent second-order set of cross-beds. Arrows: migration of dune crest and feet between 1996 and 1998.

4.2.2.1. Calculation principles, precautions and limitations. The formation periodicity of second-order surfaces can be estimated using the following formula:

$$T = S(\rho_s - \rho)/q \quad (2)$$

where T is time (days) necessary for the deposition of the sediment trapped within a second-order set of cross-beds. It corresponds to the formation periodicity of second-order surfaces, S is the vertical area (m^2) of sediment trapped within a second-order set of cross-beds, ρ_s is the sediment density, equal to 2600 kg/m^3 for a sediment composed of well sorted, medium quartz sand (typical from sector A) or poorly sorted, coarse quartz sands (typical from sector B), ρ is the water density, equal to 1000 kg/m^3, and q is the transport capacity (kg/m/day).

The vertical surface of sediment trapped between two second-order surfaces can be estimated from the seismic records (e.g., the shaded area in Fig. 5).

Precautions and limits are required regarding the presented calculation: (1) to limit underestimation of the vertical surface, the calculation should be made on the most recent, complete, second-order set of cross-beds as it is less affected by post-depositional erosion, particularly at the dune summit; (2) because second-order surfaces result from erosive processes, the amount of sediment deposited during the period between two of these events is necessarily greater than the amount preserved between two bounding surfaces, leading to an underestimation of the result; and (3) the method is valid if it is assumed that the seismic resolution is sufficient to allow the visualisation of every existing second-order surface, and that the thick signal of such bounding surfaces does not mask underlying ones.

4.2.2.2. Results. Calculations have been made for dunes, the bounding surfaces of which are clearly visible on seismic sections, enabling a good estimation of the vertical area of sediment deposited within the most recent second-order sedimentary units (Table 1). Dunes j and i SE, located in sector B, and dunes q and t, located in sector A, have been considered.

Total load transport capacities necessary for the calculation are derived from the current measurements made at station CA, using Bagnold's formula modified by Yang (1986) and van Rijn's formulas (1985, 1986).

Table 1
Formation periodicity of second-order discontinuities in dunes i SE, j, q and t calculated for mean hydrodynamic conditions (type 1) and SW ([1]) or NE ([2]) wind-driven conditions (type 2)

Sector	Dunes		Formation periodicity (days)	
	Name	Height [m]	Type 1 conditions	Type 2 conditions
A	q	6.5	116	35[1]–40[2]
	t	5.8	166	50[1]–57[2]
B	j	7.8	109	33[1]–37[2]
	i SE	11.0	223	68[1]–77[2]

The transport capacities have been calculated considering two types of hydrodynamic conditions: (type 1) mean conditions, i.e., neap to spring tides associated with a mean wind regime, and (type 2) wind-driven conditions, i.e., neap tides combined with permanent SW or NE winds. Mean conditions (type 1) are encountered when considering the entire period of the current measurement with 84% SW winds and 16% NE winds; wind-driven conditions (type 2) are observed from 1 to 4 October (SW winds), and 4 to 5 October (NE winds) (Fig. 2). Under type 1 conditions, the total load transport capacity is equal to 1100 kg/m/day. Under type 2 conditions, the total load transport capacity is equal to 3200 and 3600 kg/m/day, respectively, from 1 to 4 October, and 4 to 5 October.

The time elapsed between the formation of two second-order surfaces varies according to the dune type and hydrodynamic conditions (Table 1). For type 2 conditions, the formation periodicity is estimated as a minimum of 33–77 days (1.1–2.5 months). However, such conditions, with permanent wind-driven currents, cannot realistically be expected to occur over such a long period. Currents induced by moderate winds cannot explain the formation of second-order surfaces. For type 1 mean conditions, the formation periodicity corresponds to a minimum period of 116–166 days (3.8–5.4 months) in sector A, and of 109–223 days (3.6–7.3 months) in sector B. These longer periodicities are closer to the occurrence of storms, which have a short duration but a high erosive potential. The period covered by the seismic records (June 1996–November 1998) is characterised by a minimum of storm surge activity. In France, one violent storm period, defined as a period where at least 20% of the French meteorological stations observed a daily maximum wind speed over 100 km/h during at least 3 days, has been identified in 1996 and 1997, and none in 1998 (Bessemoulin and Dreveton, 2003). At Sylt Island, in the North Sea (Germany), only one storm surge was recorded per year in 1996 and 1997 (Dette, 1997). During the period considered in our calculation, a good correlation is found between the occurrence of storm events and the formation periodicity of second-order surfaces. In sector A, the formation of second-order surfaces seems to result from more frequent meteorological phenomena. Storms have an homogeneous influence at the scale of the study area, because their impact is regional. However, the hydrodynamic conditions necessary for the temporary inversion of tidal peak velocity asymmetry and transport are more easily reached in sector A. In addition, the dunes, which are smaller than those in sector B, probably adapt to less energetic and shorter inversions.

4.2.2.3. Discussion. Internal bounding surfaces, similar to the second-order surfaces described in this study, have been reported for other dunes mainly located in shallow marine environments, and several hypotheses have been drawn concerning the origin of these surfaces.

Some authors state that the internal structure of dunes is mainly controlled by superimposed dunes that climb down the lee slope of still larger bedforms and produce a second-order set of cross-beds and associated bounding surfaces. This has been reported for intertidal dunes in the Bay of Fundy, where second-order surfaces are produced every one to five semi-diurnal tidal cycles (Dalrymple, 1984), and for eolian dunes (Brookfield, 1992). The latter also reported that second-order bounding surfaces occur more frequently in seasonally reversing dune systems. In the Aptian to Albian Lower Greensand, a formation deposited in a shallow marine setting, slightly dipping bounding surfaces, observed with a ground-penetrating radar, are interpreted as reactivation surfaces related to a change in tidal flow (Bristow, 1995). Allen (1980) attributed the formation of the large erosive bounding surfaces to the action of the subordinate current. These mechanisms are rejected for the present study, as the processes responsible for the formation of the second-order surfaces display a much shorter occurrence than the one we have calculated (up to one discontinuity per

month). Berné (1991) also rejected these mechanisms since the lateral extension of second-order surfaces requires a width which is much larger than the extension of superimposed dunes, and the amount of sand removed is larger than the transport capacity of the subordinate current.

In the present study, the general mechanism we suggest results from the combination of tide and currents induced by storm winds. Some studies have reported similar hypotheses. In tidal dunes, Berné (1991) invoked the episodic combination of the tidal current with an oscillatory or unidirectional current, such as wave-generated currents (e.g., the Baie de Bourgneuf and the Surtainville area in France). In Cenomanian sandstones deposited in a mid- to upper shoreface setting (Brazil), Rossetti (1997) concluded that the cross beddings, which consist of large-scale (1–3 m thick) sets with low angles (10–12°), are generated under both tidal and storm processes.

4.3. Types of architecture

Three main types of internal architecture, previously reported by Berné (1991, 2003), have been recognised in the study area. They result from distinct geometric combinations of the three types of bounding surfaces. Architectures are illustrated with examples of seismic sections acquired in 1996 and 1998.

4.3.1. Asymetric dunes with cosets

Asymetric dunes with cosets mostly correspond to the largest structures having heights greater than 6 m, such as dune j (6 m) (Fig. 5), dune i SE (10.5 m) and dune i NW (8.5 m) (Fig. 6). The superimposed dunes generally form a homogeneous pattern 1–1.5 m high, but they can morph into higher (e.g., 2–3 m high on top of dune i SE in 1998), more heterogeneous shapes. Asymmetric dunes with cosets are composed of a single thick depositional unit limited by first-order surfaces and constituted by second-

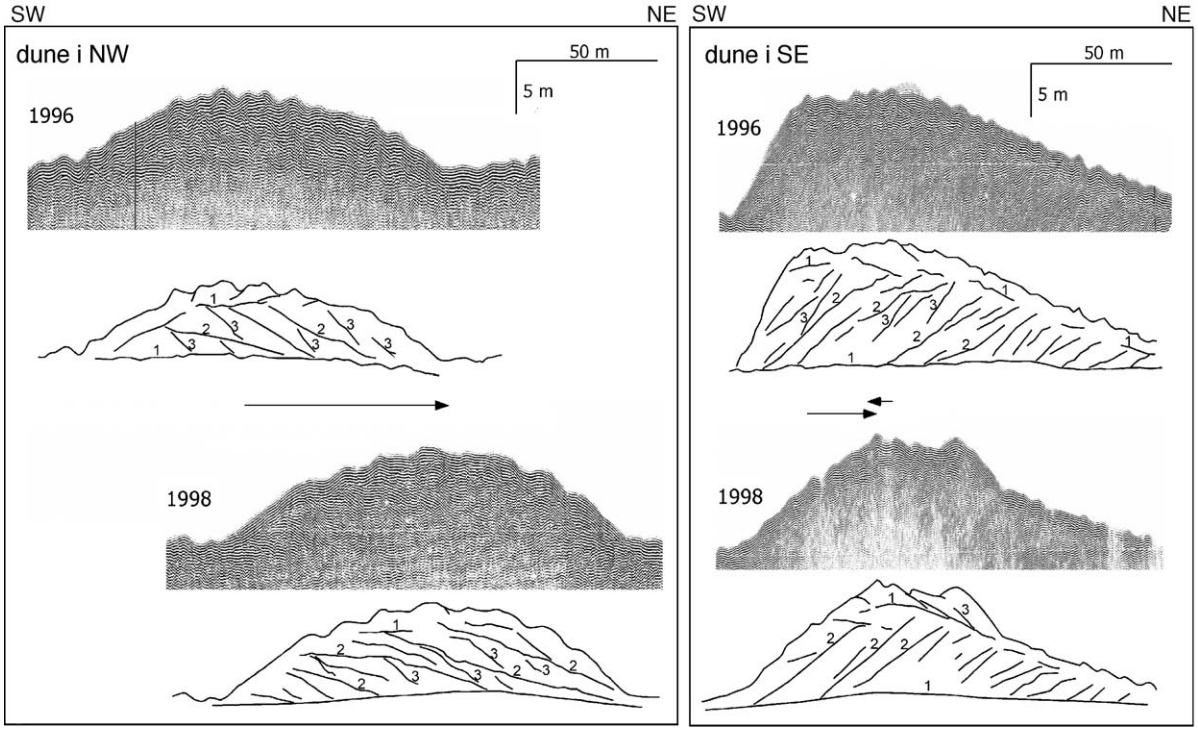

Fig. 6. Asymmetric dunes with cosets. SW–NE seismic sections perpendicular to the crest of dune i NW (profile 4, 1996; profile IV, 1998) and dune i SE (profile 9, 1996; profile IX, 1998) and their interpretation. Location of seismic sections in Fig. 9. Arrows: migration of dune crest between 1996 and 1998.

order sets of cross-beds (e.g., dunes j, i SE and i NW, Figs. 5 and 6). The thick depositional unit lies on the dune progradation surface and is truncated in its upper part by the progradation surface of superimposed dunes. Second-order sets of cross-beds are 1.7–2.1 m thick in dune j, 2.5–4.85 m in dune i SE and 1.7–3.8 m in dune i NW.

Second- and third-order surfaces dip towards the SW within dunes j and i SE, located in sector B, and towards the NE within dune i NW, located in sector A, in the direction of dune migration. Within small superimposed dunes, the internal reflectors observed may therefore dip in a direction opposite to that of the master-bedding (e.g., flood type dunes on top of dune i SE in 1998, Fig. 6). These reflectors are only observed in the uppermost unit, meaning that they are temporary and have little chance of long-term preservation.

The external morphology of these dunes is characterised by a pronounced asymmetry. Their lee side is oriented in the direction of second- and third-order surfaces. The steepness of the lee side is therefore variable with time. In 1996, the lee flanks of dune i SE and dune j, located in sector B, were as pronounced as the internal third-order reflectors and corresponded to an avalanche surface, probably inducing the development of sand flows and the deposition of cross-beds. In 1998, the lee flank did not correspond to an avalanche surface: its inclination was close to that of the second-order surfaces. Dune i NW, located in sector A, is marked by an opposite evolution: the small NE asymmetry observed in 1996 became more pronounced in 1998.

4.3.2. Dunes with mega-herringbone structures

Dunes with mega-herringbone structures display a wide range of heights, from 2.5 to 9 m. Internal organisation of these dunes is complex, as observed in dune b (8 m) and in the central part of dune i (9.5 m) (Fig. 7). It consists of an upbuilding of coset units with opposite progradation directions. The boundary between two successive sets of cross-beds consists of a second-order surface that has affected the stoss side of the dune. This second-order surface dips in the opposite direction compared to the underlying bounding surfaces. The central part of dune i was made up of three coset units in 1996 and two in 1998. Dune b is made of two cosets units. No dune with more than three coset units has been observed in the study area. Second-order sets of cross-beds are 1.5–3.1 m thick in the central part of dune i and 2.7–3.0 m thick in dune b.

Morphology can be symmetric (e.g., central part of dune i) or asymmetric (e.g., dune b). The complexity of the internal architecture is expressed in its external composite morphology, as the dune asymmetry is reversed under erosive processes, before the deposition of every coset unit.

4.3.3. Dunes with megaripple bedding units

Dunes with megaripple bedding units are observed in sand-rich sectors in dunes with moderate heights (5–6 m). These dunes consist generally of two sets of cross-beds. A basal unit, typical of asymmetric dunes with cosets or dunes with mega-herringbone structures (e.g., dune p, Fig. 8), is truncated along a horizontal reflector by an upper unit composed of a complex assemblage of small beds which dip successively in opposite directions. These complex beds are not easy to distinguish on seismic sections because of strong diffraction phenomena. The thickness of the complex beds, which is similar to the heights of superimposed dunes, indicates that the upper megaripple bedding unit of the host dunes is largely controlled by superimposed ones. In the basal unit of dune p, the thickness of second-order sets of cross-beds is 1.7–2 m. The megaripple bedding unit is not long-term preserved, and was not observed on dune p in 1996.

Like the internal architecture, the external morphology is composite. The flanks of the basal unit present an asymmetry orientated in the direction of internal bounding surface dipping. In the upper unit of the megaripple bedding, the external morphology is symmetrical.

4.3.4. Spatial distribution of the architecture types

Interpretation of the seismic profiles obtained in 1996 and 1998 has enabled us to draw synthetic maps of the dune architecture (Fig. 9) in order to analyse its spatial distribution. What is of interest in the present study is that the three types of architecture are observed within a single dune field, and sometimes within a single dune.

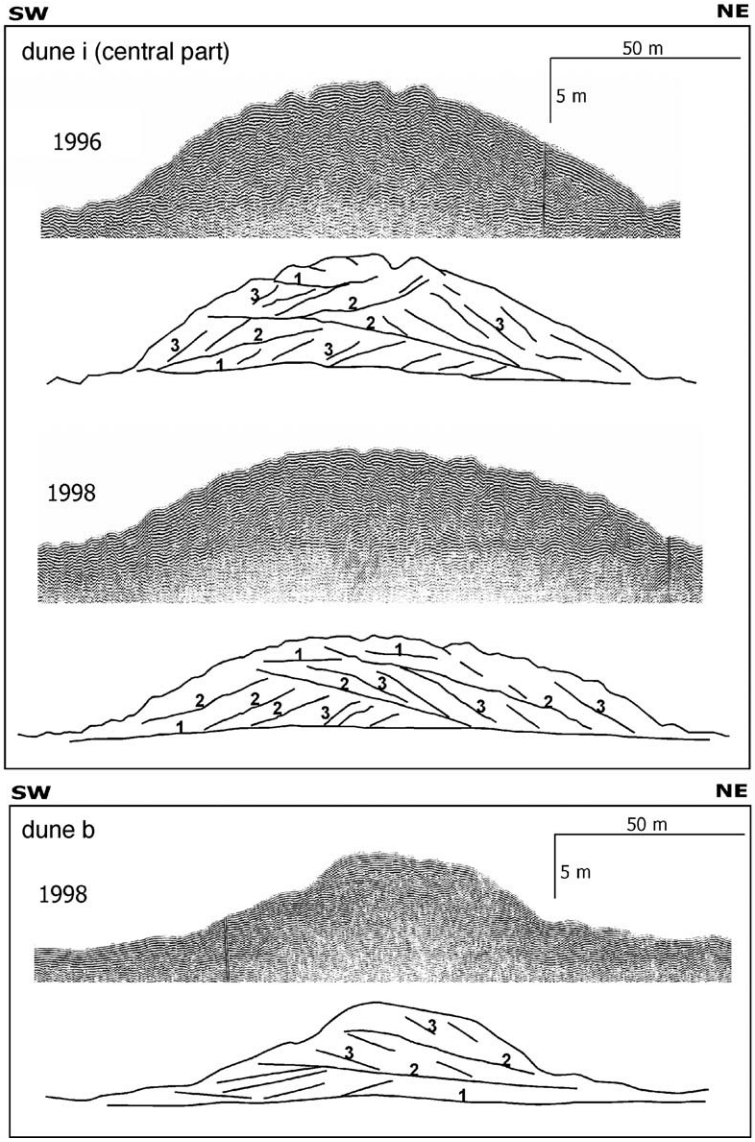

Fig. 7. Dunes with mega-herringbone structures. SW–NE seismic sections perpendicular to the crest of dune i (profile 5, 1996; profile V, 1998) and dune b (profile XII, 1998), and their interpretation. Location of seismic sections in Fig. 9.

4.3.4.1. Distribution within sectors A and B. In sector A, complex time-varying architectures are observed:

(1) In the northern part, two types of dune architecture are seen. Asymmetric dunes with cosets are the most frequently observed features. Dune asymmetry is generally towards the NE, in agreement with the dipping of internal bounding surfaces (e.g., dune i NW in 1998, Fig. 6) and the direction of long-term dune migration (Le Bot et al., 2000; Le Bot, 2001). However, some dunes present typical symmetrical units with megaripple bedding (e.g., dune p in 1998, Fig. 7). Megaripple bedding is evidence of the great density of superimposed dunes in this sand-rich area, as well as of the numerous first-order summit surfaces. However, both architectures can be observed within a given dune over time.

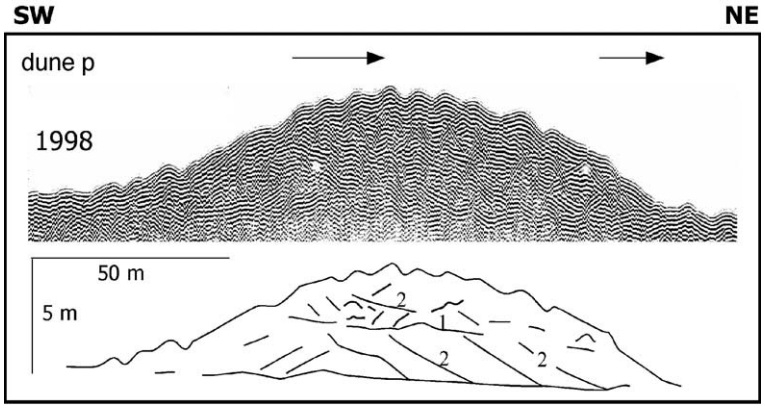

Fig. 8. Dunes with megaripple bedding units. SW–NE seismic section of dune p (profile V, 1998) and its interpretation. Location of seismic section in Fig. 9. Arrows: migration of dune crest and feet between 1996 and 1998.

(2) Dunes f, f′ and g present an architecture with mega-herringbone structures. Sometimes these dunes are asymmetric and made of cosets with a SW (1996) or NE (1998) progradational direction, implying that the dunes have been entirely rebuilt during this period. Given their small dimensions (mean heights of 2.5–4.5 m), these dunes present a rapid morphological adaptation and intensive migration rates in response to hydrodynamic fluctuations.
(3) Dunes a to e are composed of mega-herringbone structures, indicating an NE–SW alternating migration. Dunes d and e display a predominant proportion of SW-oriented second- and third-order surfaces, whereas dunes a, b and c are dominated by NE dipping bounding surfaces. This indicates a more frequent progradation of dunes towards the SW and the NE, respectively.

In sector B, dune architecture is homogeneous and constant. It consists of dunes with cosets with a SW asymmetry. Internal second- and third-order surfaces dip towards the SW in the direction of dune migration.

The portions of dunes occuring at the boundary between the two sectors (mainly dune extremities), present an architecture with mega-herringbone structures.

4.3.4.2. Dune i: a combination of the different architecture types. Dune i belongs in part to each of the two dune sectors. Its SE part (dune i SE) is located in sector B and displays the architecture characteristic of this sector: it has a strong SW asymmetry coupled with an internal architecture with cosets dipping in this direction. In the NW part of dune i (dune i NW), the architecture is of the same type, but the dune lee side and internal bounding surfaces dip towards the NE. In the central part of dune i, the architecture is typical of a symmetrical dune with mega-herringbone structures.

5. Expression of combined tide and wind processes in internal architecture and external morphology

The diversity of dune internal architecture and external morphology reveals the variable hydrodynamic and sediment transport conditions that occur in the study area.

5.1. Influence of the asymmetry of tidal current velocity

In sector A, tidal peak velocity asymmetry is low to negligible. In the northern part, the asymmetry is approximately 0.03–0.08 m/s in favour of the flood current phase. According to Pingree and Griffiths (1979), a 0.05 m/s difference between flood and ebb strength under spring tide conditions is significant in terms of sand transport and sand wave asymmetry. This is consistent with our observations. The slope of second- and third-order surfaces is mainly oriented in

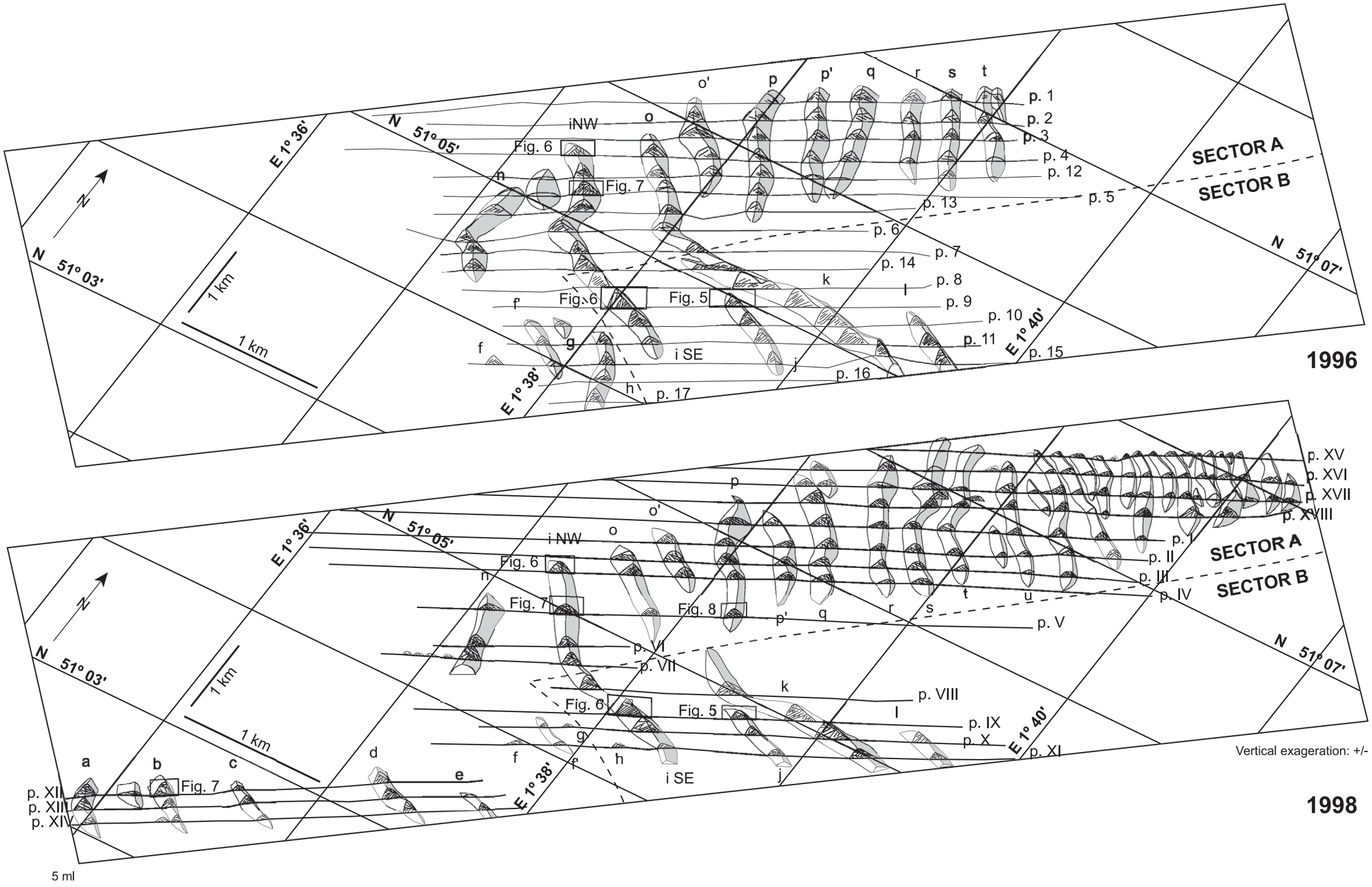

Fig. 9. Fence diagram of dune internal architecture revealed by seismic profiles in 1996 (profiles 1 to 17) and 1998 (profiles I to XVIII). General dipping directions of internal bounding surfaces and external morphology have been reported for each dune. Grey dune side is NE-oriented and white dune side is SW-oriented. Rectangles correspond to detailed seismic sections shown in Figs. 5–8. Broken line: boundary between sectors A and B.

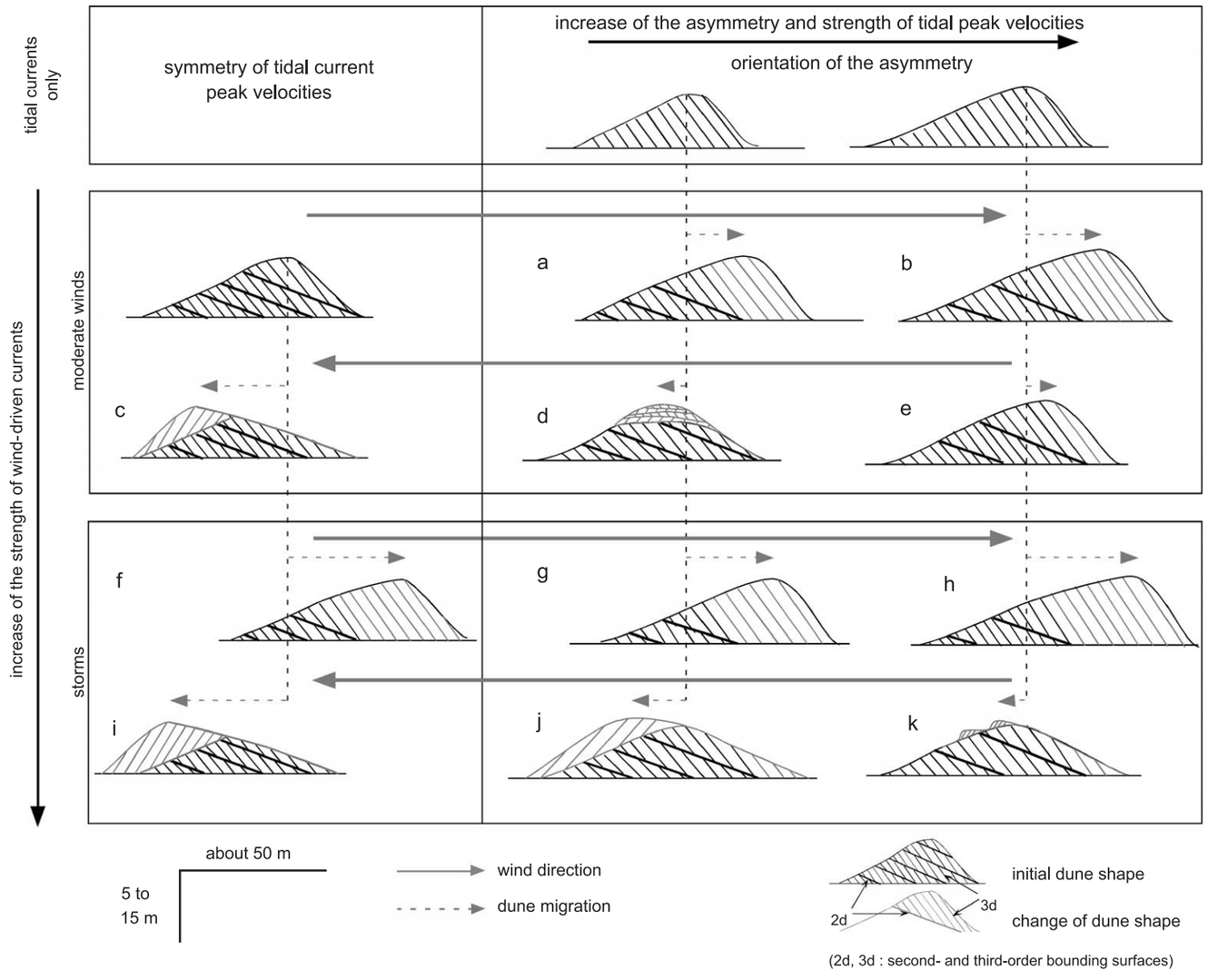

Fig. 10. Types of internal structure and external morphology of submarine dunes as a function of the asymmetry and strength of tidal peak velocities (horizontal axis) and strength of wind-driven currents (vertical axis). Types c, f and i are similar to dunes located in the southern part of sector A and at the boundary between sectors A and B; types a, d, g and j are similar to dunes located in the northern part of sector A; types b, e, h and k are similar to dunes located in sector B.

the direction of the slightly dominant flood current (i.e., the NE), and dunes generally correspond to asymmetrical dunes with cosets. Dunes a to g, located in a sediment recirculation cell (Fig. 4), demonstrate the predominance of architectures with mega-herringbone structures with complex external morphologies, indicating no preferred long-term progradational direction.

In sector B, tidal currents are strong and their peak velocity asymmetry is pronounced in favour of the ebb current. Second- and third-order surfaces within the single thick depositional unit are oriented towards the SW, in the direction of the dominant ebb current, sediment transport and dune migration.

Fig. 10 presents the types of internal architecture and external morphology expected for given tidal peak velocities and associated asymmetry, and wind-driven current velocity.

5.2. Influence of wind-driven currents

5.2.1. Moderate winds

In sector A, fluctuations in sediment transport direction and rate are directly correlated with fluctuations in the wind direction. Most dunes temporarily progradate in the direction of the tidal current phase reinforced by wind-driven currents (schemes a and c, Fig. 10). The best examples are dunes a to g located in the gyre and the central portion of dune i located at the boundary between sectors A and B. In the northern part, dune migration can cease but not be reversed. The abundant superimposed dunes display frequent progradational reversals indicating their adaptation to fluctuations of instantaneous currents. As a result, an upper symmetrical unit with megaripple bedding of alternating progradation direction temporarily forms (scheme d, Fig. 10).

In sector B, when moderate NE winds blow, the SW tidal residual transport is enhanced, resulting in thicker and/or more frequently formed sets of cross-beds (scheme b, Fig. 10). Moderate SW winds induce the decrease of SW tidal residual sediment transport but not the reversal of sediment transport direction. Dunes display the same internal architecture and external morphology as in the absence of wind, but the sets of cross-beds are temporarily thinner and/or cross-beds form less frequently. Migration of the dunes will also slow down (scheme e, Fig. 10).

5.2.2. Storm winds

In the northern part in sector A, under a SW regime, increased sediment transport rates cause an intensification of dune migration toward the NE, resulting in a thickening of the set of cross-beds and/or more numerous cross-beds (schemes f and g, Fig. 10). Under NE winds, an increase in current strength and sediment transport will result in the reversal of the progradational direction of host dunes and superimposed dunes (schemes i and j, Fig. 10). This phenomenon will lead to the formation of a new second-order surface on the dune stoss side, a new set of cross-beds dipping towards the opposite (SW) direction, and mega-herringbone structures.

In sector B, under NE winds, the lee flank is an avalanche surface, the migration accelerates, and the set of cross-beds thickens and/or cross-beds form more frequently (scheme h, Fig. 10). Under SW winds, non-reversal of tidal currents can occur during neap tides and sediment is either no longer transported or is only slightly transported towards the NE. Dune architecture and asymmetry are not modified, but the lee and stoss sides of the dune and its top are somewhat affected (scheme k, Fig. 10). The lee flank of the dunes is eroded, forming a new second-order surface. Eroded sediment is transported towards the NE and contributes to the feeding of superimposed dunes, reversing their progradation in the direction of sediment transport. Once the event stops, superimposed dunes recover their residual tidal polarity (towards the SW) and the slope of the lee flank is increased through sand-flow supply. When storm-driven currents occur, the greatest effects are to stop the dune migration and/or reverse the migration of the highest point of the dune towards the NE.

5.3. Illustration from the modifications observed from 1996 to 1998

Between 1996 and 1998, the internal architecture of the dunes presents some modifications of variable importance:

(1) Dunes f, f′ and g (sector A) have been completely rebuilt: the asymmetry of their external shape and internal sets of cross-beds was oriented towards the SW in 1996 and towards the NE in 1998.

Table 2
Regimes of SW and NE winds between 1974 and 1998 (data source: Météo-France)

Periods	NE winds		SW winds	
	N 20°–40°	N 350°–80°	N 200°–220°	N 170°–260°
1974–1982	9.3%	18.4%	13.2%	30.3%
1985–1995	5.8%	14.3%	11%	30.7%
1996–1998	5.6%	17.1%	17.1%	34%

(2) In the northern part of sector A, units of megaripple bedding disappeared between 1996 and 1998, and were replaced by fully developed coset units with a NE asymmetry. Between 1996 and 1998, dune migration was mainly towards the NE (e.g., 70 m for dunes i NW and q), increasing dune asymmetry in this direction.

(3) In sector B, the architecture has not changed and no significant dune migration has been recorded (e.g., only a few metres towards the SW for dune j, Fig. 5). Most modifications observed concern dune asymmetry. Between 1996 and 1998, large amounts of sediment were eroded from the lee flanks of dunes k and i SE, resulting in less steepness. Eroded sediments were partly deposited on the top and stoss side of host dunes: they have fed the superimposed dunes causing an increase in their dimension (especially height) and a reversal of their progradational direction towards the NE.

Observed architectural modifications consisted of either the formation of NE dipping second- and/or third-order surfaces (sector A), or the erosion of dune structures located on the SW sides of dunes (sector B). They suggest strong and/or frequent NE orientated currents during the 1996–1998 period. Compared to previous longer periods, the wind regime between 1996 and 1998 was characterised by an increase in SW winds (Table 2): N170–260° winds occurred 34% of the time (17.1% from N200–220°), and N350–80° ones 17.1% of the time (5.6% from N20–40°). This variation alone could have caused longer and more frequent periods of NE dune migration (sector A) or decreased SW dune migration (sector B), resulting in the architecture modifications observed.

6. Comparison with dunes from other shelf areas

6.1. Architecture and hydro-sedimentary processes

Large-scale cross-bedding displays strong similarities between dunes even if they are from shelf areas with different types of dominating currents (tidal, oceanic, wind- and/or swell-driven) (Flemming, 1988). According to Flemming, "The only non-ambiguous argument against a tidal setting is the absence of lunar cycles in the cross-bedded sets". We suggest that there is a correlation between architecture types and driving hydro-sedimentary processes.

Asymmetric dunes with cosets have been reported previously by Berné et al. (1988) in the area of Surtainville in the English Channel (northern France), where the hydrodynamic setting is similar to that observed in sector B, with a tidal peak velocity asymmetry of 0.4 m/s at 1.4 m above the seabed. Berné et al. (1988) proposed that this architecture results mainly from the tidal dynamics, except for the second-order surfaces formed in the case of an episodic combination of tide and storm (waves) processes.

Dunes with mega-herringbone structures are observed only in environments where non-tidal processes act. They were first described by Berné et al. (1993) in the Gironde Estuary (southwestern France), where the polarity inversion of second- and third-order reflectors is attributed to the alternation of flood- and ebb-dominated periods, related to the seasonal changes of river flow regimes. In the present study, the hydrodynamic agent combined with tides (moderate to strong winds) is different but leads to the same effects (inversion of currents and sediment transport, architecture with mega-herringbone structures). Dunes with mega-herringbone structures could also be expected to be observed in the Torres Strait (northeastern Australia) and in the Bay of Arcachon (southwestern France), where Harris (1989, 1991) and Thauront et al. (1996), respectively, observed reversal of subtidal dune asymmetries caused by seasonally wind-driven currents.

From the stability diagram of Allen (1980), which is based on the quantitative relation between tidal current velocity asymmetry and internal architecture of dunes, class IVA dunes are predicted in sector B and class VI dunes in the northern part of sector A. The predicted internal structures present geometries similar to those

observed in the study area (asymmetric dunes with cosets and dunes with megaripple units), underlining the fact that tidal current velocity asymmetry is the main parameter driving dune architecture. In the study area, however, the genetic processes differ strongly: the current velocity asymmetry is not "purely" tidal as proposed by Allen (1980), but rather results from combined tide- and wind-driven processes. The action of these time-fluctuating processes explains why the architecture type of the dunes studied often varies over time.

6.2. Architecture and dune dimensions

Dune dimension also is an important parameter affecting internal architecture, because smaller dunes can adapt much more rapidly to sediment transport fluctuations. In Allen's model, based on small intertidal ripple observations, the internal structures result from the alternation of flood and ebb phases, whereas the very large dunes from the study area react to less frequent, more energetic events. According to Dalrymple and Rhodes (1995), simple small to medium dunes display internal structures completely different from those of large to very large compound dunes in which the effect of superimposed dunes is pronounced.

6.3. Thickness of second-order sets of cross-beds

The architecture types in the study area are typical of combined tide- and wind-driven processes. As was noticed for internal bounding surfaces, the different types of dune architectures display strong geometric similarities with structures observed in dunes from other shelf environments, even though processes and dune dimensions may differ. This implies that a study based only on a geometric description of internal structures only will not allow determination of the hydrodynamic environment where dunes occur. This has important implications for the reconstitution of ancient depositional environments.

A better discriminant criteria may be the characteristics of the second-order surfaces. The formation periodicity of these bounding surfaces and the thickness of the second-order sets of cross-beds seem to be typical of specific hydrodynamic agents and resulting genetic processes, and dune dimensions. Second-order sets of cross-beds are 1.5–4.85 m thick in the present study (2.65 m on average) for very large dunes (4–12.5 m high) and 5–10 m thick in Berné et al. (1988) for very large dunes (3–7.5 m high), 0.1–1 m thick in Allen (1980) for intertidal ripples, 0.77–1.19 m thick in Dalrymple (1984) for medium intertidal dunes (0.81 m high on average), 1–3 m thick for Cenomanian dunes in Rossetti (1997), and some tens of cm up to about 15 m thick for asymmetric large to very large Aptian to Albian dunes in Bristow (1995). In the present study, the clearest relationship is observed between the maximum thickness of second-order sets of cross-beds and the dune height. The higher the dune, the thicker the second-order sets of cross-beds, as also observed from the above mentioned values. In the study area, the thickness of second-order sets of cross-beds is larger in asymmetric dunes with cosets than in dunes with mega-herringbone structures, and in sector B than in sector A. This indicates that tidal peak velocity asymmetry is the main parameter influencing the thickness of second-order sets of cross-beds. In purely tidal environments, the smaller thicknesses are caused by shorter, semi-diurnal cyclicities. In the Surtainville area, where the tidal current velocity asymmetry and dune heights are similar to those observed in our study area, the larger thicknesses of second-order sets of cross-beds (5–10 m thick) result from less frequent episodes of sediment transport reversal and second-order surface formation induced by processes with equinox cyclicities (Berné et al., 1988).

7. Conclusions

Current measurements and sediment transport calculations have enabled us to quantify the dominant tide- and wind-driven processes affecting dune architecture. Very high resolution seismic recordings were used to analyse internal structure and external morphology of dunes. The following conclusions have been drawn:

(1) In the study area, winds induce temporary currents that can lead to the reversal of sediment transport direction and induce erosion of the seabed. These processes occur when moderate winds (>5 m/s in neap conditions) blow in sectors

with negligible asymmetry of the tidal peak current velocity (some cm/s), whereas storm winds combined with neap tides are required in sectors with strong asymmetry of the tidal peak current velocity (some tens of cm/s).

(2) Dune master-bedding consists of extensive erosive bounding surfaces with 9–11° slopes, which delimit sets of cross-beds of 1.5–4.85 m thick (2.65 m on average). These second-order surfaces are formed during storms or under weaker wind conditions, depending on the tidal peak velocity asymmetry.

(3) Three main types of dune architecture are recognised, within which internal structure and external morphology are strongly linked. "Purely" asymmetrical dunes consist of a single thick unit formed of cosets dipping in the direction of external asymmetry and dune migration. Other dunes display a symmetrical or complex external morphology, and are made of an upbuilding of mega-herringbone structures, each one having an opposite progradational direction. In sand-rich sectors, dunes may have a temporary megaripple bedding unit at the summit caused by the dynamics of the superimposed dunes.

(4) Dune architecture types highlight the various hydro-sedimentary characteristics that prevail in the study area. Tidal peak velocity asymmetry and the relative strength of wind-driven currents are the parameters which have the most important influence on dune architecture. Asymmetric dunes with cosets, observed where the tidal peak velocity asymmetry is strong, are modified only in the case of storm-induced currents, which lead to the erosion of the lee flank. Dunes with mega-herringbone structures occur in areas where the tidal peak velocity asymmetry is negligible and is reversed each time moderate winds blow, leading to frequent erosion of the dune lee and stoss sides and reversal of dune asymmetry and migration. Under the same hydrodynamic conditions, dunes with a summit unit of megaripple bedding are temporary formed when abundant superimposed small to medium dunes occur, which reverse their migration at each rapid current fluctuation.

(5) The different dune architecture types are representative of the combined tide- and wind-driven processes found in the study area. They display strong geometric similarities with structures observed in dunes from other shelf environments with different processes (e.g., dunes from the tide- and wave-dominated area of Surtainville, Berné et al., 1988; dune types IVa and V–VI, Allen, 1980; intertidal medium dunes, Dalrymple, 1984). This implies that a study based only on a geometric description of internal structures will not permit determination of the hydrodynamic environment where the dunes occur. This has important implications for the reconstitution of ancient depositional environments. A better discriminant criteria is the thickness of the second-order sets of cross-beds, which is characteristic of specific hydro-sedimentary processes and resulting transport fluxes. Dune height also has an important influence on the thickness of second-order sets of cross-beds, as height and set thickness display a clear relationship in the present study.

Acknowledgments

The authors wish to acknowkledge Pr. H. Chamley and Dr. T. Garlan for their stimulating support during the study. In addition, we thank Dr. D. Idier and Dr. G. Chapalain for discussions about hydro-sedimentary processes, and Dr. S. Philpott and Dr. B. Mahler for manuscript improvements.

We also thank reviewers, Dr. P.T. Harris and Dr. S. Berné, and Editor-in-Chief, Dr. J.T. Wells, for their valuable comments.

The study was financially supported by the French Naval Hydrographic and Oceanographic Service (SHOM) and the Council of Nord-Pas de Calais. Measurements were carried out aboard the R/V BORDA (SHOM/MHA), the R/V Côtes de la Manche and the R/V Sépia II (INSU/CNRS), the crews of which are warmly thanked.

References

Allen, J.R.L., 1980. Sand waves: a model of origin and internal structure. Sediment. Geol. 26, 281–328.

Baba, J., Komar, P.D., 1981. Measurements and analysis of settling velocities of natural quartz sand grains. J. Sediment. Petrol. 51 (2), 631–640.

Beck, C., Clabaut, P., Dewez, S., Vicaire, O., Chamley, H., Augris, C., Hoslin, R., Caillot, A., 1991. Sand bodies and sand transport paths at the English Channel–North Sea border: morphology, hydrodynamics and radioactive tracing. Oceanologica Acta 11, 111–121.

Berné, S., 1991. Architecture et dynamique des dunes tidales. PhD thesis, Univ. Lille 1, France, 295 pp.

Berné, S., 2003. Offshore sands. In: Middleton, G.V. (Ed.), Encyclopedia of Sediments and Sedimentary Rocks. Kluwer Academic Publishing, Dordrecht, pp. 493–499.

Berné, S., Auffret, J.P., Walker, P., 1988. Internal structure of subtidal sand waves revealed by high-resolution seismic reflection. Sedimentology 35, 5–20.

Berné, S., Allen, G., Auffret, J.P., Chamley, H., Durand, J., Weber, O., 1989. Essai de synthèse sur les dunes hydrauliques géantes tidales actuelles. Bull. Soc. Géol. Fr. 6, 1145–1160.

Berné, S., Castaing, P., Le Drezen, E., Lericolais, G., 1993. Morphology, internal structure, and reversal of asymmetry of large subtidal dunes in the entrance to Gironde Estuary (France). J. Sediment. Petrol. 63 (5), 780–793.

Bessemoulin, P., Dreveton, C., 2003. Wind storms over France during the 20th century. French IGBP-WCRP News Letter 15, June 2003, 41–45.

Bristow, C., 1995. Facies analysis in the Lower Greensand using ground penetrating radar. J. Geol. Soc. (Lond.) 152, 591–598.

Brookfield, M.E., 1977. The origin of bounding surfaces in ancient eolian sandstones. Sedimentology 24, 303–332.

Brookfield, M.E., 1992. Eolian systems. In: Walker, R.G., James, N.P. (Eds.), Facies Models. Response to Sea Level Change. Geological Association of Canada, St. Johns, pp. 143–156.

Burton, B.W., 1977. Etude d'un champ d'ondulations de sable à l'extrême sud-ouest du banc Sandettié. Rev. Hydrogr. Int. Monaco LIV (2), 51–66.

Dalrymple, R.W., 1984. Morphology and internal structure of sandwaves in the Bay of Fundy. Sedimentology 31, 365–382.

Dalrymple, R.W., Rhodes, R.N., 1995. Estuarine dunes and bars, chapter 13. In: Perillo, G.M.E. (Ed.), Geomorphology and Sedimentology of Estuaries, Developments in Sedimentology 53, Elsevier, Amsterdam, pp. 359–422.

Dette, H.H., 1997. Evaluation of long term dune recession data. Coastal Dynamics' 97, Plymouth, pp. 10.

Dyer, K.R., 1986. Coastal and Estuarine Sediment Dynamics. Wiley, Chichester, 342 pp.

Flemming, B.W., 1988. Pseudo-tidal sedimentation in a non-tidal shelf environment (Southeast African continental margin). In: De Boer, P.L., Van Gelder, A., Nio, S.D. (Eds.), Tide-Influenced Sedimentary Environments and Facies. D. Reidel Publishing, Utrecht, pp. 167–180.

Grochowski, N.T.L., Collins, M.B., Boxall, S.R., Salomon, J.C., Breton, M., Lafite, R., 1993. Sediment transport pathways in the Eastern English Channel. Oceanol. Acta 16 (5–6), 531–537.

Harris, P.T., 1989. Sandwave movement under tidal and wind-driven currents in a shallow marine environment: adolphus Channel, northeastern Australia. Cont. Shelf Res. 9 (11), 981–1002.

Harris, P.T., 1991. Reversal of subtidal dune assymetries caused by seasonnally reversing wind-driven currents in Torres Strait, northeastern Australia. Cont. Shelf Res. 11 (7), 655–662.

Harris, P.T., Pattiaratchi, C.B., Collins, M.B., Dalrymple, R.W., 1995. What is a bedload parting? Spec. Publ. Int. Assoc. Sedimentol. 24, 3–18.

Houbolt, J.J.H.C., 1968. Recent sediments in the southern bight of the North sea. Geol. Mijnb. 47 (4), 245–273.

Idier, D., 2002a. Modèle de courants de marée pour l'étude de la dynamique des dunes sous-marines dans le détroit du Pas-de-Calais. Study Report no. 004/02-338 EPSHOM/CH/GG/NP, SHOM, 68 pp.

Idier, D., 2002b. Dynamique des bancs et dunes de sable du plateau continental: observations in-situ et modélisation numérique. PhD thesis, Institut National Polytechnique de Toulouse, France, 314 pp.

Idier, D., Ehrhold, A., Garlan, T., 2002. Morphodynamique d'une dune sous-marine du détroit du pas de Calais. C. R. Geosci. 334, 1079–1085.

James, C., Guennoc, P., Harrison, M., Le Bot, S., Philpott, S., Vinchon, C., Bee, E., Simien, F., Janjou, D., Garlan, T., Trentesaux, A., Mahieux, G., Briet, D., Augris, C., 2002. GEOSYNTH: a synthesis of the geology and sediments of the Dover Strait and its hinterland. British geological survey commissioned report. CR/02/078, 36 pp. +CD-ROM.

Jelgersma, S., 1979. Sea-level changes in the north Sea basin. In: Oele, E., Schüttenhelm, R.T.E., Wiggers, A.J. (Eds.), The Quaternary History of the North Sea. Acta Univ. Upps. Annum Quingentesimum celebrantis, Uppsala, pp. 233–248.

Johnson, M.A., Kenyon, N.H., Belderson, R.H., Stride, A.H., 1982. Sand transport. In: Stride, A.H. (Ed.), Offshore Tidal Sand, Processes and Deposits. Chapman & Hall, London, pp. 58–94.

Jones, S., Jago, C.F., Prandle, D., Flatt, D., 1994. Suspended sediment dynamics: measurement and modelling in the Dover Strait. In: Beven, K.J., Chatwin, P.C., Millbank, J.H. (Eds.), Mixing and Transport in the Environment. Wiley, Chichester, pp. 183–201.

Kenyon, N.H., Belderson, R.H., Stride, A.H., Johnson, M.A., 1981. Offshore tidal sand-banks as indicators of net sand transport and as potential deposits. In: Nio, S.D., Schüttenhelm, R.T.E., Van Weering, T.C.E. (Eds.), Holocene Marine Sedimentation in the North Sea Basin. Blackwell, London, pp. 257–268.

Le Bot, S., 2001. Morphodynamique de dunes sous-marines sous influence des marées et des tempêtes. Processus hydro-sédimentaires et enregistrement. Exemple du Pas-de-Calais. PhD thesis, Univ. Lille 1, France, 301 pp.

Le Bot, S., Trentesaux, A., Garlan, T., Berné, S., Chamley, H., 2000. Influence des tempêtes sur la mobilité des dunes tidales dans le détroit du Pas-de-Calais. Oceanol. Acta 23 (2), 129–141.

Miller, M.C., McCave, I.N., Komar, P.D., 1977. Treshold of sediment motion under unidirectional currents. Sedimentology 24, 507–527.

Pingree, R.D., Griffiths, D.K., 1979. Sand transport paths around the British Isles resulting from M2 and M4 tidal interactions. J. Mar. Biol. Assoc. U.K. 59, 497–513.

Prandle, D., 1993. Year-long measurements of flow through the Dover Strait by H.F. Radar and acoustic Doppler current profilers (ADCP). Oceanol. Acta 16 (5–6), 457–468.

Rossetti, D.F., 1997. Internal architecture of mixed tide- and storm-influenced deposits: an example from the Alcântara Formation, northern Brazil. Sediment. Geol. 114, 163–188.

Salomon, J.C., Breton, M., Guegueniat, P., 1993. Computed residual flow through the Dover Strait. Oceanol. Acta 16 (5–6), 449–455.

SHOM, 1968. Courants de marée dans la Manche et sur les côtes françaises de l'Atlantique. Service Hydrographique et Océanographique de la Marine, Paris, 287 pp.

Smith, D.E., 1988. Morphological development of the Sandettié South Falls gap: a degeneration ebb dominated tidal passage in the southern North Sea. In: De Boer, P.L., Van Gelder, A., Nio, S.D. (Eds.), Tide-Influenced Sedimentary Environments and Facies. D. Reidel Publishing, Utrecht, pp. 51–64.

Thauront, F., Berné, S., Cirac, P., 1996. Evolution saisonnière des dunes tidales dans le bassin d'Arcachon, France. C. R. Acad. Sci. (Paris) 323 (IIa), 411–418.

Trentesaux, A., Stolk, A., Berné, S., 1999. Sedimentology and stratigraphy of a tidal sand bank in the southern North Sea. Mar. Geol. 159, 253–272.

van Rijn, L.C., 1985. Sediment Transport: Part II. Suspended Load Transport, Sediment Transport. Delft Hydraulics Laboratory, Delft, pp. 1613–1641.

van Rijn, L.C., 1986. Application of sediment pick-up function. J. Hydraul. Eng., Am. Soc. Civ. Eng. 112, 867–874.

van Veen, J., 1936. Onderzoekingen in de Hoofden. Algemene Landsdruckerij. Ministerie van Waterstaat, 's-Gravenhage, (252 pp.).

Yang, C.-H., 1986. On Bagnold's sediment transport equation in tidal marine environments and the practical definition of bedload. Sedimentology 33, 465–486.